IEEE Access
Multidisciplinary | Rapid Review | Open Access Journal

Received April 18, 2019, accepted May 7, 2019, date of publication May 22, 2019, date of current version June 26, 2019.

Digital Object Identifier 10.1109/ACCESS.2019.2918297

Bifurcation Mechanism and Stabilization of V^{2}C Controlled Buck Converter

WEI HU[1], BO ZHANG[2], (Senior Member, IEEE), AND RU YANG[3]

[1]Lab Center, Guangzhou University, Guangzhou 510006, China
[2]School of Electric Power, South China University of Technology, Guangzhou 510641, China
[3]School of Mechanical and Electrical Engineering, Guangzhou University, Guangzhou 510006, China

Corresponding author: Bo Zhang (epbzhang@scut.edu.cn)

This work was supported by the Teamwork Project of the Natural Science Foundation, Guangdong, China, under Grant 1714060000016.

ABSTRACT The V^{2}C controlled buck converter by constant-frequency pulse-width modulation in continuous conduction mode gives rise to a great variety of instability behaviors, depending on the circuit parameter values. In this paper, the discrete-time model of the regulator is built by taking a current sampling resistor into consideration. The resulting Monodromy matrix is used to investigate the bifurcation phenomenon and stabilization property. The converter shows a series of period-doubling bifurcation phenomena accordingly as the feedback amplification coefficient increases. At the same time, a couple of Floquet multipliers pass through the unit circle along the negative real axis. Therefore, it reveals the mechanism of a series of period-doubling bifurcations happened in the system from the perspective of stability. Based on Floquet theory, a sine voltage compensation method is proposed to stabilize the bifurcation and chaotic behaviors. The simulations and experimental results proved the theoretical analysis.

INDEX TERMS V^{2}C control, buck converter, period-doubling bifurcation, chaos.

I. INTRODUCTION

Switching power converters are widely employed in various applications, including emergency power supplies, photovoltaic power generation, and electric sources for personal or laptop computers, as well as vehicle drivers [1].

As a typical PWM control system, V^{2}C controlled converter takes the ripples of output voltage and inductor current as the control signals. By comparison the ripples with error comparator, the duty cycle will be adjusted to achieve the desired output voltage [2]. The control law derived from adding a feedback current to the original V^2 strategy [3], [4], which means that the manipulating method adopts summation of the peak voltage inner loop and peak current outer loop as the feedback signal. The V^2 controlled converter has the advantages of rapid responses to the load and voltage changes, fitness to the low voltage circuit and so on. Due to the small ESR of the output capacitor, slope of the inner loop signal was too small to be detected, which could result in poor disturbance rejection capabilities. Methods such as [5]–[7] are proposed to handle the issue. As a solution to the mentioned problem, the V^{2}C control strategy is proposed. With synthesize the advantages of V^2 implementation and current control strategy, the V^{2}C method offers abilities of rapid response to the step change with the load and input as well as the well anti-interference, see [2] and the references there in.

Switching power converters are strong nonlinear circuits with rich dynamical behaviors. So far, in such systems, plenty of complicated nonlinear phenomena have been observed, such as multi-equilibria [8], period-doubling bifurcation [9], Hopf bifurcation [10], quasi-periodicity [11], border collision [12], bi-stability [13] and chaos [14], [15].

The discrete-time model of V^{2}C controlled continuous conduction mode (CCM) boost converter has been built and the route to chaos has been analyzed during the variation of the circuit parameters, see [16]. The sub-harmonic oscillation behavior is illustrated and the slope compensation is introduced to control it [17]. The sub-harmonic oscillation of the power regulator affected by the ESR of the output capacitor has been investigated in [18], however, the influences of voltage feedback coefficient on stability property is not considered, nor did control method of stabilizing the converter system is addressed. The mechanism of bifurcation and chaos belong to the V^{2}C controlled buck converter are still open problems.

The associate editor coordinating the review of this manuscript and approving it for publication was Yijie Wang.

Totally speaking, bifurcation and chaos are harmful to practical applications. With the purpose of suppressing the instability behaviors in dc-dc converters, the researchers have proposed some stabilization strategies to control chaos, such as the OGY method [19], Filter based non-invasive control [20], parameter perturbation [21], adaptive control method [22] and so on. Features of these methods lie in taking advantages of the measures such as state feedback or parameter disturbance, etc, to change the state variables, and achieve the stabilization of controlled variables. These help make control variables return to the steady period state from the chaos state. Among all the chaos control strategies, parameter perturbation method has been applied extensively due to the simplicity and high efficiency, especially a sine wave voltage perturbation.

In order to explore the nonlinear behaviors of V²C controlled converter in a further step, solve some system unstable behaviors in projects, and guide some applications in practical engineering, this paper takes buck converter as the object, computes the system Monodromy matrix, reveals the system stable characteristics, and then analyzes the unstable behaviors when the coefficient of error amplifier changes, and uses the sine voltage compensation to stabilize the system and extends the stability boundary.

The outline of the paper is as follows. The mathematical model of V²C manipulated buck converter is introduced in Section II. Section III describes the switching points and the Mondromy matrix of the closed-loop system. Section IV is devoted to investigations of Mechanism of period-doubling bifurcation and chaos exhibit in the power stage. In Section V, the stabilization control strategy is performed. The next section gives experimental results for verification of the proposed model. Section VII contains the conclusions.

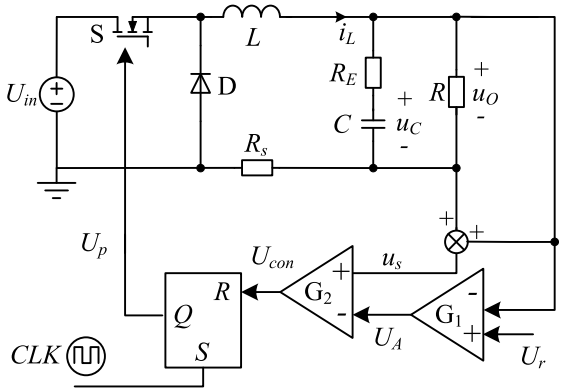

FIGURE 1. V²C controlled buck converter.

II. DISCRETE-TIME MODEL OF CLOSED-LOOP CONVERTER

Block diagram of V²C manipulated buck converter is as Fig. 1 shows, where G_1, R_e, R_s and U_r are feedback amplification factor, ESR of output capacitor, sampled resistor and reference voltage, respectively.

Supposing the output capacitance is chosen large enough that the voltage u_C can be considered constant. Hence, the output voltage is given by

$$u_O = \Delta i_L R_E + u_C. \tag{1}$$

The detection voltage of the inner loop is

$$u_s = u_O + R_s i_L. \tag{2}$$

Substitution of Eq. (1) into Eq. (2), there will be

$$u_s = \Delta i_L R_E + u_C + R_s i_L. \tag{3}$$

When u_s increases to the error voltage U_A, the comparator G_2 will turns over which makes U_p changes to low level, the switch S turns off and the inductor current deceases linearly. Until the next clock pulse signal comes, it will start a new switching period.

In the buck converter, i_L denotes the inductor current, u_C denotes the capacitor voltage and they are the elements of the state variable $\boldsymbol{x} = [x_1, x_2]^T = [i_L, u_C]^T$. The mathematical model matrices are collected in TABLE 1.

TABLE 1. Mathematical model parameters of buck converter.

State Matrices	Output Matrices	S	D
$\boldsymbol{A}_1 = \begin{bmatrix} -\frac{1}{L}\left(R_s + \frac{RR_E}{R+R_E}\right) & -\frac{R}{L(R+R_E)} \\ \frac{R}{C(R+R_E)} & -\frac{1}{C(R+R_E)} \end{bmatrix}$	$\boldsymbol{B}_1 = \begin{bmatrix} \frac{U_{in}}{L} \\ 0 \end{bmatrix}$	*on*	*off*
$\boldsymbol{A}_2 = \begin{bmatrix} -\frac{1}{L}\left(R_s + \frac{RR_E}{R+R_E}\right) & -\frac{R}{L(R+R_E)} \\ \frac{R}{C(R+R_E)} & -\frac{1}{C(R+R_E)} \end{bmatrix}$	$\boldsymbol{B}_2 = \begin{bmatrix} 0 \\ 0 \end{bmatrix}$	*off*	*on*

In general, the considered closed-loop buck converter belongs to a class of Filippov systems:

$$\dot{\boldsymbol{x}} = \boldsymbol{f}(t, \boldsymbol{x}), \boldsymbol{f}(t, \boldsymbol{x}) = \begin{cases} \boldsymbol{f}^+(t, \boldsymbol{x}) \ \ if \ h(t, \boldsymbol{x}) > 0, \\ \boldsymbol{f}^-(t, \boldsymbol{x}) \ \ if \ h(t, \boldsymbol{x}) < 0. \end{cases} \tag{4}$$

where, $\boldsymbol{f}^-(t, \boldsymbol{x})$ and $\boldsymbol{f}^+(t, \boldsymbol{x})$ are two vector fields before and after the switching manifold Σ, separately.

Here the scalar function $h(t, \boldsymbol{x})$ has a nonvanishing gradient ∇h on the switching manifold

$$\Sigma = \{(t, \boldsymbol{x}) : h(t, \boldsymbol{x}) = 0\}.$$

The switching manifold Σ separates the state space of system (4) into two different regions in which the dynamic behavior of (4) is governed by different vector fields $\boldsymbol{f}^-(t, \boldsymbol{x})$ and $\boldsymbol{f}^+(t, \boldsymbol{x})$.

Therefore, the state equations of CCM buck converter are described as follows

$$\begin{aligned} \boldsymbol{f}^- &= \boldsymbol{A}_1 \boldsymbol{x} + \boldsymbol{B}_1 \\ &= \begin{bmatrix} -\frac{1}{L}\left(R_s + \frac{RR_E}{(R+R_E)}\right) i_L - \frac{Ru_C}{L(R+R_E)} \\ \frac{Ri_L - u_C}{C(R+R_E)} \end{bmatrix} + \begin{bmatrix} \frac{U_{in}}{L} \\ 0 \end{bmatrix}, \end{aligned} \tag{5}$$

$$\boldsymbol{f}^{+} = \boldsymbol{A}_2\boldsymbol{x} + \boldsymbol{B}_2 = \begin{bmatrix} -\frac{1}{L}\left(R_s + \frac{RR_E}{(R+R_E)}\right) i_L - \frac{Ru_C}{L\,(R+R_E)} \\ \frac{Ri_L - u_C}{C\,(R+R_E)} \end{bmatrix}. \quad (6)$$

The mathematical expression of V²C control strategy can be described as

$$u_s - U_A = 0. \quad (7)$$

Meanwhile

$$U_A = G_1\,(U_r - u_O)\,, \quad (8)$$

Substitute Eq. (3) and Eq. (8) into Eq. (7), we get

$$u_O + R_s i_L - G_1(U_r - u_O) = 0, \quad (9)$$

which equivalent to

$$u_O - \frac{U_r G_1 - R_s i_L}{1 + G_1} = 0. \quad (10)$$

Supposing the value of R_E is very small, if G_1 is much larger than 1, then we can say that $u_O \approx U_r$. The impacts on the stability of the converter caused by G_1 will be analyzed in detail in section III.

Eq. (10) can be rewritten as

$$u_O + \frac{R_s i_L}{1 + G_1} = \frac{U_r G_1}{1 + G_1}, \quad (11)$$

where $\frac{R_s i_L}{1+G_1}$ is larger than zero, and we have $u_O < \frac{U_r G_1}{1+G_1}$. Meanwhile, $\frac{G_1}{1+G_1}$ is definite, and we have $u_O < U_r$. Only when $G_1 \gg 1$ and $R_s \approx 0$ fulfill, $u_O \approx U_r$ is obtained. In this case, G_1 is very large and $U_r - u_O$ is relatively small, the product of them does not equal zero. As a result, U_A is greater than zero, so does u_s. Therefore, V²C control strategy functions.

In this paper, G_1 was chosen as 2, 2.5 and 20, which do not fulfill the conditions mentioned above. As a result, the output voltage u_O are less than U_r.

As $i_O = \frac{u_O}{R} \approx \frac{u_C}{R}$ and taking u_O as the controlled object, the switching surface of Eq. (10) could be rewritten as

$$h_2 = u_C + \left(i_L - \frac{u_C}{R}\right) R_E - \frac{U_R G_1 - R_s i_L}{1 + G_1} = 0. \quad (12)$$

Since $\boldsymbol{A}_1 = \boldsymbol{A}_2 = \boldsymbol{A}$ and $\boldsymbol{B}_2 = [0, 0]^T$, the iterate equations of switching points belong to CCM buck converter can be written as [23] shows:

$$e^{\boldsymbol{A}d_nT}\boldsymbol{x}(nT) + \boldsymbol{A}^{-1}(e^{\boldsymbol{A}d_nT} - \boldsymbol{I})\boldsymbol{B} = \boldsymbol{x}(nT + d_nT) \quad (13)$$

$$e^{\boldsymbol{A}d'_nT}\boldsymbol{x}(nT + d_nT) = \boldsymbol{x}[(n+1)T]. \quad (14)$$

where, d_n is the relative pulse duty cycle for the n-th rump period, i.e. for the time interval $nT < t < (n+1)T$ and $d'_n = 1 - d_n$.

Substitution of Eq. (13) into Eq. (14) yields

$$\boldsymbol{x}[(n+1)T] = e^{\boldsymbol{A}T}[\boldsymbol{x}(nT) + \boldsymbol{x}_s] - e^{\boldsymbol{A}d'_nT}\boldsymbol{x}_s, \quad (15)$$

where, $\boldsymbol{x}_s = \boldsymbol{A}^{-1}\boldsymbol{B}$.

It is clear that Eq. (15) shows the discrete-time mathematical model of CCM V²C manipulated buck converter. As thesystem enters stable mode, $x[(n+1)T]$ equals to $x(nT)$, Eq. (15) could be rewritten as

$$\boldsymbol{x}\,(nT) = \frac{e^{\boldsymbol{A}d_nT} - e^{\boldsymbol{A}d'_nT}}{\boldsymbol{I} - e^{\boldsymbol{A}d_nT}}\boldsymbol{x}_s \quad (16)$$

From the switching surface at the switching off point

$$x_2\left(1 - \frac{R_E}{R}\right) + x_1\left(R_E + \frac{R_s}{K_v + G_1}\right) = \frac{U_r G_1}{K_v + G_1} \quad (17)$$

According to Eq. (13), one obtain

$$x_2\left(1 - \frac{R_E}{R}\right) + x_1\left(R_E + \frac{R_s}{K_v + G_1}\right) = \left[\left(1 - \frac{R_E}{R}\right), \left(R_E + \frac{R_s}{K_v + G_1}\right)\right] \times (e^{\boldsymbol{A}d_nT}\boldsymbol{x}(nT) + \boldsymbol{A}^{-1}(e^{\boldsymbol{A}d_nT} - \boldsymbol{I})\boldsymbol{B}), \quad (18)$$

Therefore,

$$\frac{U_r G_1}{K_v + G_1} = \left[\left(1 - \frac{R_E}{R}\right), \left(R_E + \frac{R_s}{K_v + G_1}\right)\right] \times (e^{\boldsymbol{A}d_nT}\boldsymbol{x}(nT) + \boldsymbol{A}^{-1}(e^{\boldsymbol{A}d_nT} - \boldsymbol{I})\boldsymbol{B}). \quad (19)$$

Substitution of $\boldsymbol{x}(nT)$ from Eq. (16) into Eq. (19) yielding duty cycle d_n. As a result, the state variables $\boldsymbol{x}(nT)$ are obtained. Note that if the duty cycle d_n is 0 or 1, then the modulator will saturate, the OFF or ON state of switching tube will remains during the current switching period till next cycle begins.

III. STABILITY ANALYSIS

In a switching period, the trajectory of state variable belongs to converter forms a limit cycle in the phase space. According to Filippov theorem [24]–[27], as the maximum eigenvalue (also named Floquet multiplier) of Monodromy matrix belongs to state transition matrix in a switching period is within the unit circle, the power converter stays stable; when it is on the unit circle, the period-doubling bifurcation phenomenon will happen in the system; otherwise, the system is unstable.

The local stability of the periodic solution $\boldsymbol{x}_p$ is determined by the eigenvalues (multipliers) of the Monodromy matrix $\boldsymbol{M}$. The Monodromy matrix $\boldsymbol{M}$ is found by solving the variation equation:

$$\dot{\boldsymbol{M}}\,(t) = D_x\boldsymbol{f}^{\pm}\left(\boldsymbol{x}_p(t)\right)\boldsymbol{M}\,(t)\,, \boldsymbol{M}\,(0) = \boldsymbol{I}\ for\ 0 < t < dT \quad (20)$$

and

$$\dot{\boldsymbol{M}}\,(t) = D_x\boldsymbol{f}^{\pm}\left(\boldsymbol{x}_p(t)\right)\boldsymbol{M}\,(t)\,, \boldsymbol{M}^{+} = \boldsymbol{S}\cdot\boldsymbol{M}^{-} \quad for\ dT < t \le T, \quad (21)$$

with

$$\boldsymbol{S} = \boldsymbol{I} + \boldsymbol{P}^{-},\ \boldsymbol{M}^{\pm} = \boldsymbol{M}\,(dT \pm 0) = \lim_{t \to dT \pm 0}\boldsymbol{M}\,(t)\,, \quad (22)$$

where,

$$\boldsymbol{P}^{-} = \left.\frac{\left(\boldsymbol{f}^{+}-\boldsymbol{f}^{-}\right)\boldsymbol{n}^{T}}{\frac{\partial h}{\partial t}+\boldsymbol{n}^{T}\boldsymbol{f}^{-}}\right|_{\substack{=\boldsymbol{x}_p \\ =dT}},$$
$$\boldsymbol{f}^{\pm} = \lim_{t\to dT\pm 0}\boldsymbol{f}^{\pm}\left(\boldsymbol{x}\left(t\right)\right).$$

Here $D_x\boldsymbol{f}^{\pm}\left(\boldsymbol{x}_p(t)\right)$ is the Jacobian matrix, $\boldsymbol{S}$ is the saltation matrix, $\boldsymbol{I}$ is the unit matrix and $\boldsymbol{n}^T = \frac{\partial h(t,\boldsymbol{x})}{\partial \boldsymbol{x}}$, $\dot{\boldsymbol{M}}\left(t\right) = \frac{d\boldsymbol{M}(t)}{dt}$.

Hence, the Monodromy matrix $\boldsymbol{M}(T)$ for the considered system is determined by

$$\boldsymbol{M}\left(T\right) = \boldsymbol{\Phi}_2 \cdot \boldsymbol{S} \cdot \boldsymbol{\Phi}_1 = e^{\boldsymbol{A}(1-d)T} \cdot \boldsymbol{S} \cdot e^{\boldsymbol{A}dT} \tag{23}$$

where, $\boldsymbol{\Phi}_1 = e^{\boldsymbol{A}dT}$ and $\boldsymbol{\Phi}_2 = e^{\boldsymbol{A}(1-d)T}$ are the transition matrices.

From the switching surface of the regulator, normal vector could be given by

$$\boldsymbol{n} = \begin{bmatrix} R_E + \dfrac{R_s}{1+G_1} \\ 1 - \dfrac{R_E}{R} \end{bmatrix}, \tag{24}$$

the derivative of switching surface with respect to time t is:

$$\frac{\partial h(t,\boldsymbol{x})}{\partial t} = 0, \tag{25}$$

and then the following equations can be obtained:

$$\left(\boldsymbol{f}^{+}-\boldsymbol{f}^{-}\right)\boldsymbol{n}^{T} = \begin{bmatrix} -\left(R_E + \dfrac{R_s}{1+G_1}\right)\frac{U_{in}}{L} & -\dfrac{U_{in}\left(1-R_E/R\right)}{L} \\ 0 & 0 \end{bmatrix}, \tag{26}$$

$$\boldsymbol{n}^{T}\boldsymbol{f}^{-} = \begin{bmatrix} R_E + \dfrac{R_s}{1+G_1} & 1-\dfrac{R_E}{R} \end{bmatrix} \cdot \left\{ \begin{bmatrix} -\dfrac{i_L}{L}\left(R_s + \dfrac{RR_E}{R+R_E}\right) - \dfrac{Ru_C}{L(R+R_E)} \\ \dfrac{Ri_L - u_C}{C(R+R_E)} \end{bmatrix} + \begin{bmatrix} \dfrac{U_{in}}{L} \\ 0 \end{bmatrix} \right\}, \tag{27}$$

Substitution of the former four equations into Eq. (22) yielding the expressions of saltation matrix $\boldsymbol{S}$. As a result, the Monodromy matrix $\boldsymbol{M}(T)$ in the whole period is obtained.

Provided that the entire system will exhibit period-4 bifurcation behavior, the trajectory of the state crosses the switching surfaces four times during two switching periods. The resulting Monodromy matrix is as follows:

$$\boldsymbol{M}(2T) = \boldsymbol{S}_4 \cdot \boldsymbol{\Phi}_4 \cdot \boldsymbol{S}_3 \cdot \boldsymbol{\Phi}_3 \cdot \boldsymbol{S}_2 \cdot \boldsymbol{\Phi}_2 \cdot \boldsymbol{S}_1 \cdot \boldsymbol{\Phi}_1. \tag{28}$$

where, $\boldsymbol{S}_i$, $i = 1, 2, 3, 4$ are the saltation matrices of the switching surfaces; $\boldsymbol{\Phi}_i$ are the transition matrices.

To calculate the state variables at the switching instant, we could follow the procedure similar to Eqs. (12) and (13). Based on the calculations, the values of the state variables will be obtained, as well as the switching matrices and transition ones. As a result, the eigenvalues of $\boldsymbol{M}(2T)$ will be determined, which leads to the indication of the period-4 bifurcation. However, the method used in the paper could not predicts the occurrence of chaos.

Apparently, R_s and R_E will influence both $(\boldsymbol{f}^{+}-\boldsymbol{f}^{-})\boldsymbol{n}^T$ and $\boldsymbol{n}^T\boldsymbol{f}^{-}$. Furthermore, they would have impacts on saltation matrix $\boldsymbol{S}$ and Monodromy matrix $\boldsymbol{M}$. Thus, Both the resistors have to be contained in the proposed mathematical model of the converter.

TABLE 2. The circuit parameters of V^{2}C controlled buck convector.

Parameter	Value	Parameter	Value
U_{in}	$8V$	L	$200\mu H$
f	$15kHz$	C	$1800\mu F$
d	$[0,1]$	U_r	$5V$
R_s	0.15Ω	R_E	0.026Ω
R	3Ω		

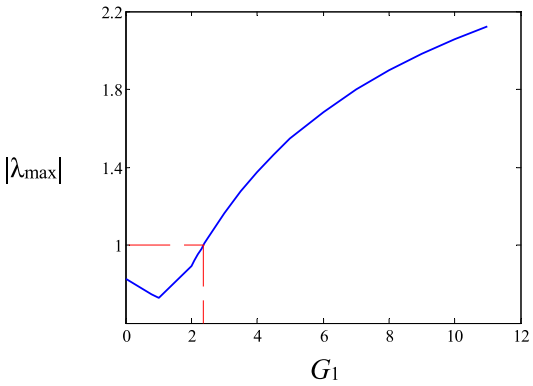

FIGURE 2. Evolution diagram of the maximum Floquet multiplier.

IV. MECHANISM OF THE BIFURCATION AND CHAOS

In order to facilitate analysis, one adopts the parameters shown in TABLE. 2. From Eq. (15), we can calculate the Floquet multiplier of Monodromy matrix $\boldsymbol{M}$, whose evolutions and loci diagram are plotted in Fig. 2 and Fig. 3, separately. The resulting bifurcation diagram is illustrated in Fig. 4. The stable borderline between the period-2 bifurcation and period-one orbit is found by setting the maximum Floquet multiplier to 1:

$$\max\left|\lambda_{\boldsymbol{M}}\right| = 1. \tag{29}$$

By combining Eqs. (23) and (29), we can work out that $G_1 = 2.240$, and at this time instant, the eigenvalues are -1.000 and 0.5924, respectively. Therefore, a multiplier passes through the unit circle from the negative real line, the other stays within the unit circle. At this point, the period-doubling bifurcation occurs.

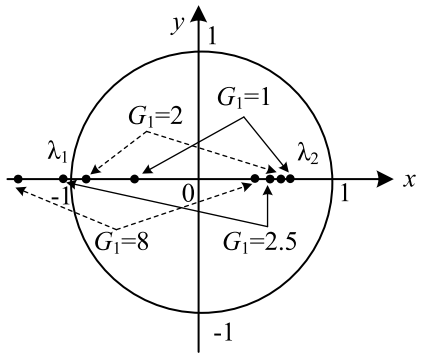

FIGURE 3. Multipliers loci for $G_1 \in [1, 8]$.

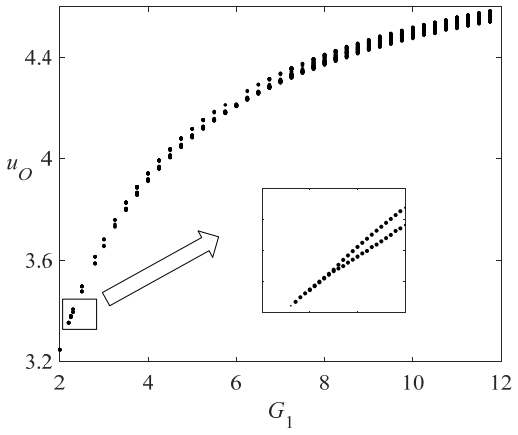

FIGURE 4. Bifurcation diagram of the converter.

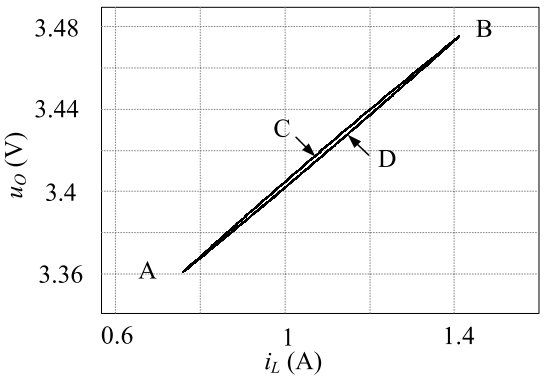

FIGURE 5. Phase portrait of a stable period one orbit with $G_1 = 2$.

A. PERIOD-ONE

The system works in the stable period one state when $G_1 = 2$. The phase portrait of $i_L - u_O$ and simulation spectrums of i_L are depicted in Fig. 5 and Fig. 6, respectively. The Floquet multipliers are 0.9260 and 0.6052. The equilibrium points of subsystems S_1 and S_2 are $E_1(2.67, 8)$ and $E_2(0, 0)$, respectively. When the system switches periodically between two subsystems, the dynamical behaviors of the system are composed of them. Meanwhile, the periodic switching would form two interfaces. One of them is the switching condition, also namely the switching surface h_2; the other would be the periodic clock signal T.

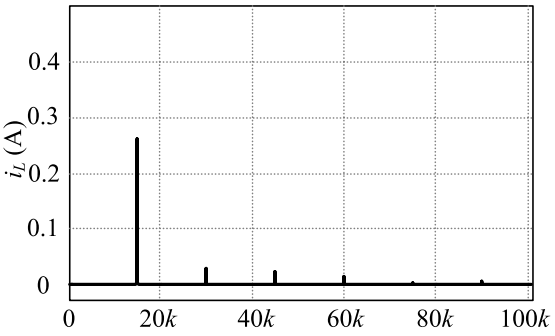

FIGURE 6. Simulation frequency spectrums of the ripples of i_L with $G_1 = 2$.

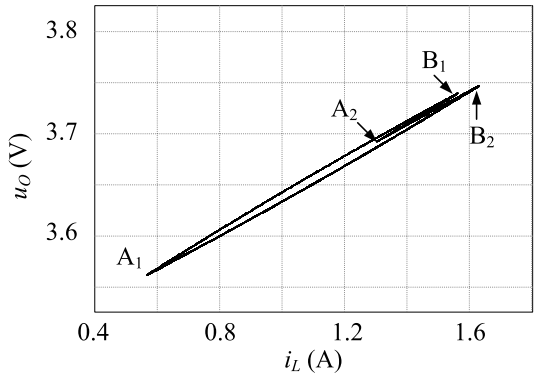

FIGURE 7. Phase portrait of a period doubling orbit with $G_1 = 2.5$.

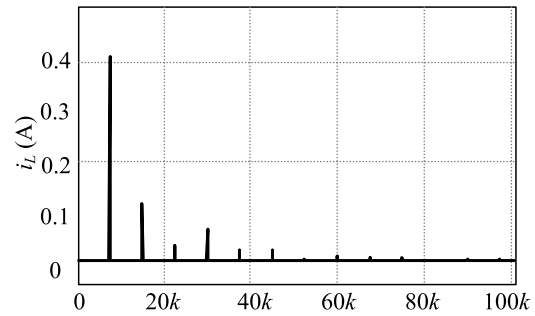

FIGURE 8. Simulation frequency spectrums of the ripples of i_L with $G_1 = 2.5$.

B. PERIOD-DOUBLING

Since $G_1 = 2.5$, the Floquet multipliers are 1.074 and 0.5798. The maximum Floquet multiplier is greater than 1 and period doubling bifurcation takes place, as shown in Fig. 7. The simulation spectrums of i_L is illustrated in Fig. 8. Suppose the system starts when $t = 0$ with starting point A_1. The system first runs in the mode with switch S is on. In this time interval, the trajectory of the converter is shown as the curve of A_1-B_1, which has the equilibrium point of $E_1(2.67, 8)$. After time interval of $t = d_1 T$, the state variables reaches the switching surface h_2 and turns off the switch. Therefore, the curve of $B_1 - A_2$ depicts the state trajectory in the second time interval with equilibrium point $E_2(0, 0)$. At the time $t = T$, the next switching period starts. The resulting state trajectories are illustrated as the curves of $A_2 - B_2$ and $B_2 - A_1$. At time

instant of $t = 2T$, the state variables return to A_1. By repeating these procedures continuously, the period-doubling oscillation is formed.

C. CHAOS

As the feedback coefficient G_1 continues to increase, period-doubling bifurcation correspondingly happens in the system. When G_1 increases to a certain value, the system trajectory generates the chaos phenomenon. The phase diagram is presented in Fig. 9 when $G_1 = 20$, and the Floquet multipliers are 2.454 and 0.3801, separately. The resulting simulation spectrums of i_L is depicted in Fig. 10.

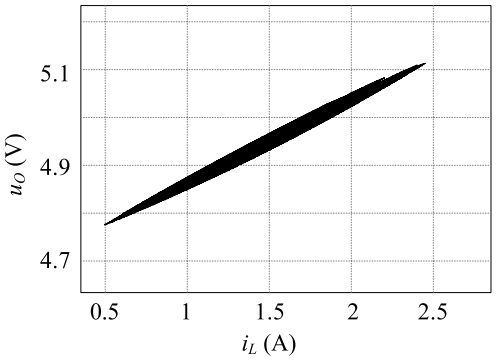

FIGURE 9. Phase portrait of chaotic orbit with $G_1 = 20$.

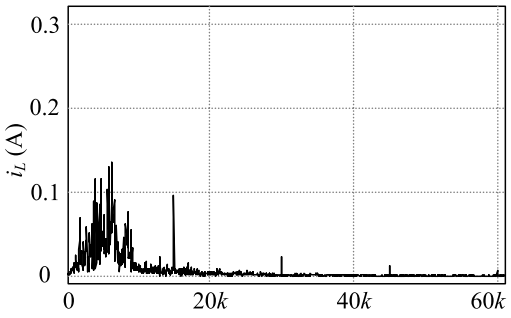

FIGURE 10. Simulation frequency spectrums of the ripples of i_L with $G_1 = 20$.

From the above analysis, it can be concluded that the V²C controlled buck converter has significant nonlinear behaviors with the change of the circuit parameters. This paper just only analyses how the change of feedback ratio G_1 affects the unstable behaviors of the converter. Likewise, the method introduced in this paper is available to study the impacts of other circuit parameters, e.g. U_r and U_{in}, on the system dynamic behavior.

V. STABILIZATION CONTROL

In order to stabilize the unstable behaviors of the system, the stabilization control strategy is proposed. A sinusoidal signal U_e which has the same frequency of the switching frequency f is added on U_r, thus ∇h_2 and saltation matrix $\boldsymbol{S}_1$ will be changed, which makes the maximum eigenvalue of Monodromy matrix lies in the unit circle and expands the stability boundary. Resulting from which, the bifurcation and the chaotic phenomena of the system are controlled successfully [21].

TABLE 3. Stable borderline as max $|\lambda_{Me}| = 1$.

G_1	$a_{\min}$	d_eT	$i_L(d_eT)$	$u_C(d_eT)$
2.240	0	$2.9584e^{-5}$	1.4565	3.3808
5	$0.2791e^{-2}$	$3.6004e^{-5}$	1.7026	4.1149
8	$0.4376e^{-2}$	$3.8535e^{-5}$	1.7928	4.4043
11	$0.4599e^{-2}$	$3.9806e^{-5}$	1.8366	4.5496

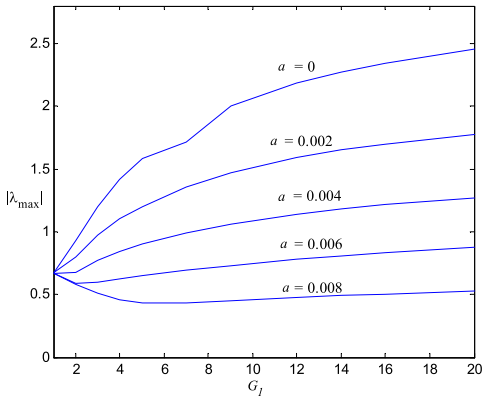

FIGURE 11. Evolution diagram of multipliers with different a.

Additive sinusoidal signal U_e takes the form of $a\sin(2\pi ft)$, then the resulting reference voltage after being compensated is:

$$U_{re} = U_r + U_e = U_r + a\sin(2\pi ft). \tag{30}$$

The switching surface and its derivative equation can be expressed as follows

$$h_e = u_C + \left(i_L - \frac{u_C}{R}\right)R_E - \frac{[U_r + a\sin(2\pi ft)]\,G_1 - R_s i_L}{1+G_1} = 0, \tag{31}$$

$$\nabla h_e = \frac{2a\pi fG_1\cos(2\pi fd_eT)}{1+G_1}. \tag{32}$$

The saltation matrix can be shown as follows

$$\boldsymbol{S}_{e1} = \boldsymbol{I} + \frac{(\boldsymbol{f}_+ - \boldsymbol{f}_-)\boldsymbol{n}_e^T}{\boldsymbol{n}_e^T\boldsymbol{f}_- + \nabla h_e}. \tag{33}$$

where, $\boldsymbol{n}_e = \begin{bmatrix} R_E + \frac{R_s}{1+G_1} \\ 1 - \frac{R_E}{R} \end{bmatrix}$.

Hence, the Monodromy matrix is:

$$\boldsymbol{M}_e = \boldsymbol{S}_{e2}\cdot\boldsymbol{\Phi}_{eoff}\cdot\boldsymbol{S}_{e1}\cdot\boldsymbol{\Phi}_{eon} = \boldsymbol{\Phi}_{eoff}\cdot\boldsymbol{S}_{e1}\cdot\boldsymbol{\Phi}_{eon}. \tag{34}$$

From Eq. (34), we can figure out the minimum boundary value $a_{\min}$ of the system stabilization. The value is shown in Table 3. Meanwhile, The evolution diagram of multipliers with different feedback coefficient a is depicted in Fig. 11.

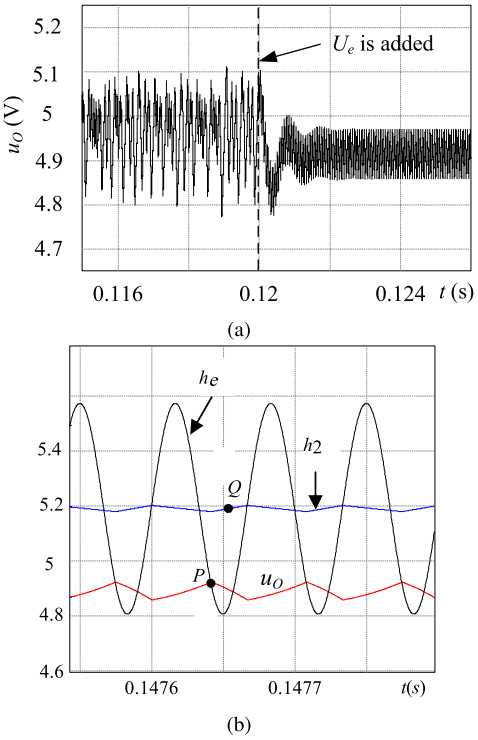

FIGURE 12. The phase diagram of the output voltage waveform. (a) Transient response of the output voltage. (b) Output voltage and the switching surfaces.

An extra sinusoidal signal $U_e = 0.1\sin(2\pi ft)$ is imposed on reference voltage U_r at the time $t = 0.12s$. From simulation result Fig. 12, the output voltage u_O reaches the stable state of period one within 20 switching periods. The transient responses of the output voltage and switching surface are shown in Fig. 13. The values of the switching points and Floquet multipliers are as collected in Table. 4.

TABLE 4. The Floquet multiplier when $a = 0.1$.

a	G_1	$i_L(d_eT)$	$u_C(d_eT)$	λ_{Me}	$\max\|\lambda_{Me}\|$
0.1	20	1.8745	4.6778	$0.78 \pm 0.39i$	0.8751

It is clear that the compensation makes the output voltage of the converter u_O intersects with the point P of the positive half period of h_e, rather than intersects with the switching surface h_2 at point Q, which shortens the distance between the switching balance point $\boldsymbol{x}(d_eT)$ and the switching surface h_2, then the duty cycle of the converter is reduced. Therefore, the time interval of adding energy in the system decreases slightly and the system achieves the stable orbit of period one.

VI. EXPERIMENTAL RESULTS

Experimental waveforms are described to verify the theoretical analysis. The experimental schematic is illustrated in Fig. 13.

It is clear that the ESR of the output capacitor influence the stability property of the entire system greatly. Therefore, the ESR is illustrated in Fig. 1, independently. However, in real applications, the ESR belongs to the output capacitor will not actually implemented.

The experimental waveforms are shown in Fig. 14. The top of every diagram is the reference voltage U_r, the middle waveforms are the output voltage u_O, inductor current i_L and duty cycle d, the lowest are the pulse signals CLK. The experiments show that as the feedback factor G_1 increases constantly, the V²C controlled buck converter will enters into the period-doubling state from the stable period one, and then it will double continuously until chaos. After the sinusoidal signal compensation $U_e = 0.1\sin(2\pi ft)$ is injected to U_r,

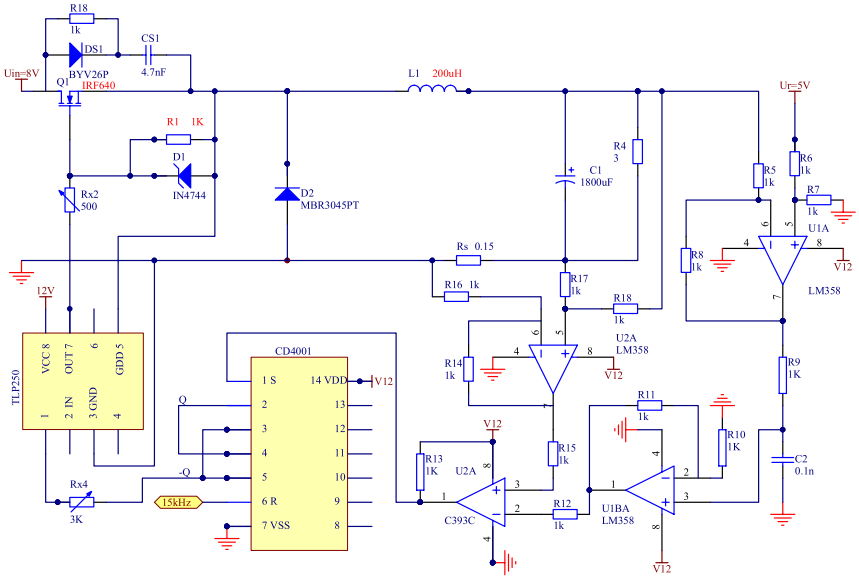

FIGURE 13. The circuit diagram of V²C controlled buck converter.

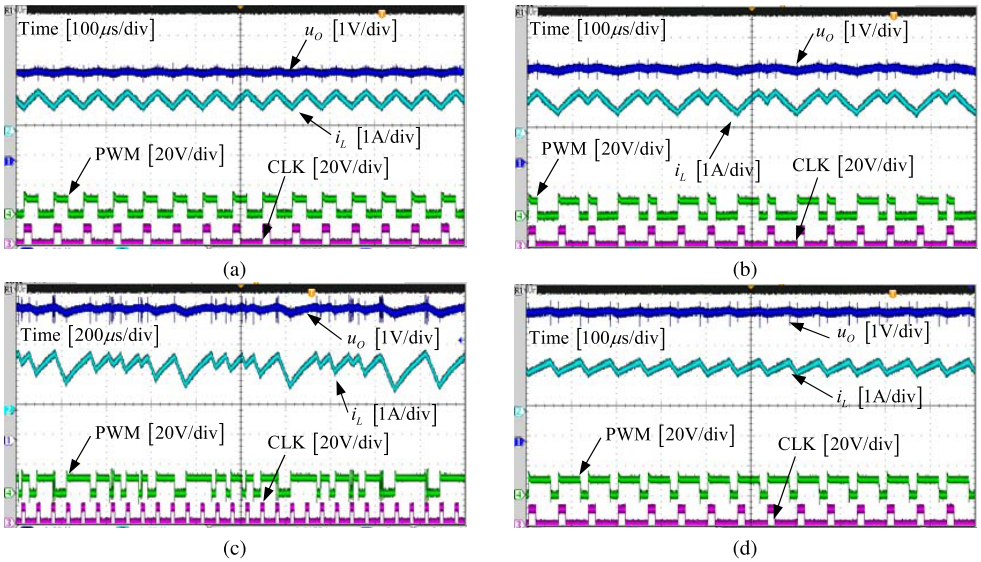

FIGURE 14. Experimental waveforms of V^{2}C controlled buck converter. (a) The waveforms of period-one when $G_1 = 2$. (b) Period-doubling bifurcation when $G_1 = 2.5$. (c) Chaos when $G_1 = 20$. (d) Controlling chaos to stable period-1 when $a = 0.2$.

the V^{2}C controlled buck converter is stabilized into stable state of period-one.

It can be seen that the output voltage and inductor current are smaller than the simulation results, owing to the ignorance of the parasitic components such as equivalent series resistance. The same reason, the state deviations is generated, which is within acceptable limits. In summary, bifurcation behaviors of theoretical analysis and experimental waveforms were found to correlate well with each other.

VII. CONCLUSION

The V^{2}C controlled buck converter has some outstanding advantages, such as the fast load transient response, which can be applied in some industrial environment with low voltage and heavy load changes. As the feedback factor G_1 increases, the output voltage of the system gets close to the reference voltage gradually, but in the same time, the period-doubling bifurcation also occurs, which will cause the system turns to be unstable. That is to say, the system will show the period-doubling bifurcation and the fourth period bifurcation and even comes into chaos from the stable period one. The theory of Monodromy matrix reveals why the period-doubling bifurcation takes place in the system. With the increase of G_1, a characteristic multiplier of the Monodromy matrix passes through the unit circle from the negative half plane in the coordinate axis, and then the period-doubling bifurcation occurs. According to this principle, under the premise of not affecting the system steady-state error, use the sinusoidal voltage to compensate the reference voltage, to decrease the duty ratio of the system slightly, to shorten the length of obtaining energy and to stabilize the converter's output signal into the first periodic orbit from bifurcation or chaos. This method extends the stable region of the system and improves the stability of the system, which is beneficial for promotion and application of V^{2}C control strategy in the industrial field.

REFERENCES

[1] R. Redl and J. Sun, "Ripple-based control of switching regulators—An overview," *IEEE Trans. Power Electron.*, vol. 24, no. 12, pp. 2669–2680, Dec. 2009.

[2] G. Zhou, J. Xu, and J. Wang, "Constant-frequency peak-ripple-based control of buck converter in CCM: Review, unification, and duality," *IEEE Trans. Ind. Electron.*, vol. 61, no. 3, pp. 1280–1291, Mar. 2014.

[3] D. Gorder and W. R. Pelletier, "V^2 architecture provides ultra fast transient response in switch mode power supplies," in *Proc. HFPC Conf.*, 1996, pp. 19–23.

[4] D. Gorder, "Switching regulators," U.S. Patent 5 770 940, Jun. 23, 1998.

[5] J. Li and F. C. Lee, "Modeling of V^2 current-mode control," *IEEE Trans. Circuits Syst. I, Reg. Papers*, vol. 57, no. 9, pp. 2552–2563, Sep. 2010.

[6] C.-H. Tsai, S.-M. Lin, and C.-S. Huang, "A fast-transient quasi-V^2 switching buck regulator using AOT control with a load current correction (LCC) technique," *IEEE Trans. Power Electron.*, vol. 28, no. 8, pp. 3949–3957, Aug. 2013.

[7] K. Y. Cheng, F. Yu, F. C. Lee, and P. Mattavelli, "Digital enhanced V^2-type constant on-time control using inductor current ramp estimation for a buck converter with low-ESR capacitors," *IEEE Trans. Power Electron.*, vol. 28, no. 3, pp. 1241–1252, Mar. 2013.

[8] M. Spinetti-Rivera, J. M. Olm, D. Biel, and E. Fossas, "Bifurcation analysis of a Lyapunov-based controlled Boost converter," *Commun. Nonlinear Sci. Numer. Simul.*, vol. 18, no. 11, pp. 3108–3125, 2013.

[9] W. Hu, B. Zhang, R. Yang, and D. Qiu, "Dynamic behaviours of constant on-time one-cycle controlled boost converter," *IET Power Electron.*, vol. 11, no. 1, pp. 160–167, Dec. 2018.

[10] P. Deivasundari, G. Uma, and R. Poovizhi, "Analysis and experimental verification of Hopf bifurcation in a solar photovoltaic powered hysteresis current-controlled cascaded-boost converter," *IET Power Electron.*, vol. 6, no. 4, pp. 763–773, Apr. 2013.

[11] C.-C. Fang, "Bifurcation boundary conditions for current programmed PWM DC–DC converters at light loading," *Int. J. Electron.*, vol. 99, no. 10, pp. 1365–1393, 2012.

[12] S. Maity, "Dynamics and stability issues of a discretized sliding-mode controlled DC-DC buck converter governed by fixed-event-time switching," *IEEE Trans. Circuits Syst. I, Reg. Papers*, vol. 60, no. 6, pp. 1657–1669, Jun. 2013.

[13] X. Zhang, B. Bao, H. Bao, Z. Wu, and Y. Hu, "Bi-stability phenomenon in constant on-time controlled buck converter with small output capacitor ESR," *IEEE Access*, vol. 6, pp. 46227–46232, 2018.
[14] Y. Wang, R. Yang, B. Zhang, and W. Hu, "Smale horseshoes and symbolic dynamics in the buck–boost DC–DC converter," *IEEE Trans. Ind. Electron.*, vol. 65, no. 1, pp. 800–809, Jan. 2018.
[15] P. Deivasundari, G. Uma, and S. Ashita, "Chaotic dynamics of a zero average dynamics controlled DC-DC cuk converter," *IET Power Electron.*, vol. 7, no. 2, pp. 289–298, Feb. 2014.
[16] B. C. Bao and J. P. Xu, "Dynamical behavior of V2C control boost converter," *J. Southwest Jiaotong Univ.*, vol. 18, no. 1, pp. 32–38, Jan. 2010.
[17] C. Mi, J. Xu, G. Zhou, and Y. Jin, "On the stability of V2C controlled boost converter in continuous conduction mode," in *Proc. IPEMC*, May 2009, pp. 1300–1304.
[18] J. Cortés, V. Švikovic, P. Alou, J. A. Oliver, and J. A. Cobos "Design and analysis of ripple-based controllers for buck converters based on discrete modeling and Floquet theory," in *Proc. COMPEL*, Salt Lake City, UT, USA, Jun. 2013, pp. 1–9.
[19] E. Ott, C. Grebogi, and J. A. Yorke, "Controlling chaos," *Phys. Rev. Lett.*, vol. 64, pp. 1196–1199, Mar. 1990.
[20] W.-G. Lu, L.-W. Zhou, Q.-M. Luo, and X.-F. Zhang, "Filter based non-invasive control of chaos in buck converter," *Phys. Lett. A*, vol. 372, no. 18, pp. 3217–3222, 2008.
[21] Y. Zhou, C. K. Tse, S. S. Qiu, and F. C. Lau, "Applying resonant parametric perturbation to control chaos in the buck DC/DC converter with phase shift and frequency mismatch considerations," *Int. J. Bifurcation Chaos*, vol. 13, no. 11, pp. 3459–3471, 2003.
[22] J. Moreno-Valenzuela, "Adaptive anti control of chaos for robot manipulators with experimental evaluations," *Commun. Nonlinear Sci. Numer. Simul.*, vol. 18, no. 1, pp. 1–11, 2013.
[23] S. Samanta, S. Mukhopadhyay, and R. Sheehan, "Discrete-time simulation of a peak current controlled DC/DC buck converter using modal decomposition," *IET Power Electron.*, vol. 4, no. 6, pp. 642–650, Jul. 2011.
[24] Z. T. Zhusubaliyev, E. A. Soukhoterin, V. N. Rudakov, Y. V. Kolokolov, and E. Mosekilde, "Bifurcations and chaotic oscillations in an automatic control relay system with hysteresis," *Int. J. Bifurcation Chaos*, vol. 11, no. 5, pp. 1193–1231, 2001.
[25] D. Giaouris, S. Banerjee, B. Zahawi, and V. Pickert, "Stability analysis of the continuous-conduction-mode buck converter via Filippov's method," *IEEE Trans. Circuits Syst. I, Reg. Papers*, vol. 55, no. 4, pp. 1084–1096, May 2008.
[26] S. Maity, D. Giaouris, S. Banerjee, T. K. Bhattacharya, B. Zahawi, and V. Pickert, "Control of bifurcations in power electronic DC-DC converters through manipulation of the saltation matrix," in *Proc. PhysCon*, Potsdam, NY, USA, Sep. 2007, pp. 1–5.
[27] A. F. Filippov, "Differential equations with discontinuous right-hand side," *Amer. Math. Soc. Transl.*, vol. 42, no. 2, pp. 199–231, 1964.

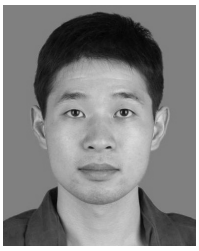

WEI HU was born in Ningxiang, China, in 1980. He received the B.S. and M.S. degrees from the College of Electrical and Information Engineering, Hunan University, Changsha, China, in 2003 and 2006, respectively, and the Ph.D. degree in power electronics from the South China University of Technology, Guangzhou, China, in 2017.

Since 2006, he has been with Guangzhou University, Guangzhou. He has authored or coauthored over 30 papers. His current research interests include the modeling and the nonlinear control of power converters, and stability analysis of dc–dc converters.

BO ZHANG (M'03–SM'15) was born in Shanghai, China, in 1962. He received the B.Sc. degree in electrical engineering from Zhejiang University, Hangzhou, China, in 1982, the M.S. degree in power electronics from Southwest Jiaotong University, Chengdu, China, in 1988, and the Ph.D. degree in power electronics from the Nanjing University of Aeronautics and Astronautics, Nanjing, China, in 1994.

He is currently a Professor with the School of Electric Power, South China University of Technology, Guangzhou, China. He has authored or coauthored over 450 papers. He held 102 patents. He has authored eight monographs. His research interests include the nonlinear analysis and the control of power supplies and ac drives.

RU YANG was born in Changsha, China, in 1971. She received the M.S. degree in electronic engineering from the Guangdong University of Technology, Guangzhou, China, in 1999, and the Ph.D. degree in power electronics from the South China University of Technology, Guangzhou, China, in 2007.

Since 1999, she has been with Guangzhou University, Guangzhou, where she is currently a Professor with the School of Mechanical and Electrical Engineering. She has authored over 50 published technical papers. Her current research interests include time and frequency-domain analysis of power electronics, chaotic switching techniques, electromagnetic interference, and chaos detection.